# Dynamical adiabatic theory of atomic collisions: Charge exchange in collisions of $He^{2+}$ with H(1$s$)

T. P. Grozdanov*
*Institute of Physics, University of Belgrade, Pregrevica 118, 11080 Belgrade, Serbia*

E. A. Solov'ev
*Bogoliubov Laboratory of Theoretical Physics, Joint Institute for Nuclear Research, 141980 Dubna, Moscow region, Russia*
(Received 21 August 2015; published 7 October 2015)

Interference effects in slow $He^{2+} + H(1s)$ charge-exchange collisions are analyzed within the framework of the dynamical adiabatic theory of atomic collisions. Analytic continuation of the dynamical adiabatic scaled-energy eigenvalues into the complex plane of internuclear separation $R$ for the $HeH^{2+}$ system is used to identify relevant branch points responsible for both radial and rotational nonadiabatic transitions leading to the electron capture process. The calculated electron capture probabilities are compared with the results of hyperspherical close-coupling calculations.

DOI: 10.1103/PhysRevA.92.042701 PACS number(s): 34.20.Cf, 34.70.+e, 34.10.+x

## I. INTRODUCTION

The adiabatic approach to slow atomic collisions is valid for impact energies up to the maximum of the corresponding inelastic cross section (∼10 KeV/nucleon). This interval covers many processes occurring in the natural world, including ionized stellar atmospheres and TOKAMAK fusion plasmas. Alternative approaches are different versions of numerical close-coupling calculations. However, in all versions, the questions of where and why inelastic transitions occur have no answer. That is why all of them belong to computational rather than theoretical physics.

In the adiabatic approximation the total wave function is expanded in terms of adiabatic eigenstates of the quasimolecule formed during the collision. However, this approach raises a well-known problem (for a review see [1]), related to the fact that the molecular basis is not compatible with the physical boundary conditions because the electrons are asymptotically attached to moving centers. In a full quantum-mechanical treatment, the problem can be resolved by employing the hyperspherical adiabatic approach proposed by Macek [2]. It has been widely used in the past, including for the $He^{2+} + H$ system [3], which we shall treat as an example in the present work.

In semiclassical theory, where the motion of the nuclei is treated classically, in order to ensure the Galilean invariant theory, it is necessary to attach so-called electron translational factors to each of the molecular adiabatic basis functions [1]. Another approach is to use the *nonstationary scaling of length* [4], which has also found useful applications in the theory of electron-atom (molecule) collisions [5] and the interaction of atoms and molecules with radiation fields [6,7]. In this method the colliding nuclei are at rest, but their effective charges are time dependent, and additional dynamical interactions occur in the electronic Hamiltonian. For the case of one electron and two nuclei, we have studied in our recent works [8,9] the instantaneous eigenvalues of this Hamiltonian (which will be referred to as *dynamical adiabatic eigenvalues*) as functions of the internuclear separation $R$ both on the real axes [8] and in the complex $R$ plane [9].

In the present work we show how the analytic continuations of dynamical adiabatic eigenvalues and corresponding branch points between them can be used to describe inelastic transitions, in particular the charge-exchange process

$$He^{2+} + H(1s) \to He^{+}(n = 2) + H^{+}. \tag{1}$$

The plan of this article is as follows. In Sec. II we review the basics of standard adiabatic and dynamical adiabatic theory of transition in systems with slowly varying time-dependent interactions. Specific cases of a two-state system and a three-body problem (one electron and two nuclei) are discussed in some detail. In Sec. III, as an example of the two-state problem, the $\sigma$-$\pi$ rotational transitions in the united-atom limit are discussed from the standpoint of adiabatic and dynamical adiabatic approaches. Section IV contains our main results of the application of the dynamical adiabatic theory to description of the process (1). The conclusions of our work are given in Sec. V.

## II. ADIABATIC AND DYNAMICAL ADIABATIC APPROXIMATIONS

In quantum physics the adiabatic approximation was proposed in 1928 by Born and Fock [10] for the Schrödinger equation

$$i\hbar\frac{\partial}{\partial t}\Psi(\mathbf{r},t) = \hat{H}(vt)\Psi(\mathbf{r},t) \tag{2}$$

while slowly varying in time Hamiltonian $\hat{H}(vt)$. They proved that in the limit $v \to 0$ the population of eigenstates of the instantaneous Hamiltonian, $\hat{H}(\tilde{\tau})\varphi_i(\mathbf{r},\tilde{\tau}) = E_i(\tilde{\tau})\varphi_i(\mathbf{r},\tilde{\tau})$, does not change ($\tilde{\tau} = vt$); that is, the adiabatic states $\varphi_i(\mathbf{r},\tilde{\tau})$ are the correct states of zeroth order in the adiabatic approximation. For the time-dependent Schrödinger equation (2) these states take the form

$$\Psi_i(\mathbf{r},t) = \varphi_i(\mathbf{r},\tilde{\tau})\exp\left(\frac{i}{\hbar}\int^t E_i(vt')dt'\right). \tag{3}$$

In 1932 Stueckelberg [11] derived the adiabatic asymptote for the probability of an inelastic transition, employing Zwaan's

*tasko@ipb.ac.rs

 

technique [12] (for details, see, e.g., Ref. [13], Sec. 47). In atomic collision theory, when the motion of the nuclei is treated classically, the electronic Hamiltonian depends on time through the internuclear distance $R(vt)$, where $v$ has the meaning of impact velocity. The adiabatic energies of the same symmetry $E_i(R)$ are different branches of the single analytic function $E(R)$ connected to each other through complex branch points $R_c$. This property follows from the implicit function theorem in complex analysis: $\Delta(E,R) = \det[\hat{H}(R) - E\hat{I}] = 0$, where $\hat{I}$ is the identity operator. According to the Zwaan method [12], the transition from initial $\varphi_i(\mathbf{r},R)$ to final $\varphi_f(\mathbf{r},R)$ adiabatic states can be obtained by analytic continuation of the adiabatic wave function (3) along the contour $C$ in the complex $R$ plane which starts at any real $R_1$ where $E(R_1) = E_i(R_1)$, goes around a complex branch point $R_c$, and ends up back on any real $R_2$ where $E(R_2) = E_f(R_2)$. This procedure is correct for an ordinary branch point $[\Delta E(R) \sim \sqrt{R - R_c}]$ with *three* Stokes lines. It is the key point of Zwaan's method. The final result for the probability of inelastic transition reads [11]

$$p_{\mathrm{if}} = e^{-2\Delta}, \tag{4}$$

where

$$\Delta = \frac{1}{\hbar}\left|\mathrm{Im}\int_C E(R)\frac{dt}{dR}dR\right| \tag{5}$$

is the Stueckelberg parameter.

Thus, the probability of an inelastic transition is determined by the integral from the real axis to the complex branch point $R_c$. Of course, during the collision, inelastic transitions occur at the real values of $R$. The physical reason for the decisive role of the complex branch points $R_c$ is the following. A branch point appears in the complex $R$ plane near a real value of $R$, where one of the energy curves $E_i(R)$ crosses the top of the barrier in the effective electron potential. Here, the adiabatic eigenstate $\varphi_i(\mathbf{r},R)$ dramatically concentrates on the top of barrier involving neighboring state $\varphi_f(\mathbf{r},R)$ to preserve the smooth behavior of the two-state subspace. As a rule, such reconstruction within the two-state subspace cannot be identified on the plot of $E_i(R)$ for real internuclear separations $R$. That is why the denotation "hidden crossing" was introduced for this connection. Hidden crossings are clearly manifested in the matrix element of nonadiabatic coupling $W_{\mathrm{if}}(R) = \langle i|d/dR|f\rangle$, which has a maximum at this point producing inelastic transitions. Thus, inelastic transitions happen whenever caustics of electron classical trajectories change their topology.

Now let us consider the mathematical aspects of hidden crossings. At the point of degeneracy of two eigenvalues $E_i(R_c) = E_f(R_c) \equiv E_c$, the Hamiltonian reduces not to a diagonal form but rather to the Jordan form. In the vicinity of $R_c$, perturbation theory with respect to a small value of $(R - R_c)$ can be used,

$$\begin{gathered}\widehat{H}(R) = \begin{pmatrix} E_c & 1 \\ 0 & E_c \end{pmatrix} + (R - R_c)\begin{pmatrix} V_{11} & V_{12} \\ V_{21} & V_{22} \end{pmatrix}, \\ V_{nm} = \mathrm{const},\end{gathered} \tag{6}$$

which gives the energies in the first approximation $E_{i,f}(R) = E_c \pm \sqrt{V_{21}(R - R_c)}$. Thus, the square-root dependence arises instead of the usual linear dependence of $\Delta E_{\mathrm{if}}(R)$ on $(R - R_c)$ at real $R$; that is, $E_i(R)$ and $E_f(R)$ are different branches of a single (multivalued) analytic function $E(R)$. The same is true for the adiabatic wave functions $\varphi_i(\mathbf{r},R)$. But the Jordan form has only one eigenvector, and to keep the orthonormalization condition at branch point $R_c$, an adiabatic wave function must have the singular factor

$$\varphi_i(\mathbf{r},R) \sim \frac{1}{\sqrt[4]{R - R_c}}, \tag{7}$$

leading to an indeterminacy at $R = R_c$, which is resolved in a different way, so that zero is obtained for the condition of orthogonality and unity is obtained for the normalization condition. As a result, the matrix element of nonadiabatic coupling $W_{\mathrm{if}}(R)$ has a pole of the first order, $W_{\mathrm{if}}(R) \approx 1/[4(R - R_c)]$, and a bell-shaped profile for real values of $R$ [see, for example, Fig. 3(b)].

The dynamical adiabatic approach has been formulated for a two-state problem in Ref. [14]. In the $n$th order of the dynamical approach the matrix elements of the time-dependent Schrödinger equation for the state vector $\mathbf{A} = [A_1, A_2]^T$,

$$i\hbar v\frac{d}{d\tilde{\tau}}\mathbf{A} = \widehat{H}_n\mathbf{A}, \quad \widehat{H}_n = \begin{pmatrix} \frac{1}{2}\Delta E_n & W_n \\ W_n^* & -\frac{1}{2}\Delta E_n \end{pmatrix}, \tag{8}$$

are connected to the lower order by the relations

$$\begin{aligned}\Delta E_n &= \sqrt{\Delta E_{n-1}^2 + 4|W_{n-1}|^2}, \\ W_n &= -i\hbar v\frac{\Delta E_{n-1}^2}{\Delta E_n^2}\frac{d}{d\tilde{\tau}}\left(\frac{|W_{n-1}|}{\Delta E_{n-1}}\right)\end{aligned} \tag{9}$$

and are obtained by transition to the eigenvector basis of the lower-order Hamiltonian $\widehat{H}_{n-1}$. The first order $(n = 1)$ corresponds to the standard adiabatic basis, where $\Delta E_1$ is the splitting of adiabatic potential energies and $W_1$ is the matrix element of nonadiabatic coupling. The physical reason for such a transformation is that the higher $n$ is, the weaker the coupling at $v \to 0$ is since $W_n \sim v^n$.

For the three-body system consisting of one electron plus two nuclei (moving along the straight-line trajectories, $\mathbf{R} = \mathbf{b} + \mathbf{v}t$, with the impact parameter $\mathbf{b}$ and relative collision velocity $\mathbf{v}$) the dynamical adiabatic approximation has been studied in Refs. [8,9]. After scaling the electron coordinates with $R(t)$, transforming to the molecular (rotating with internuclear axis) frame, and separating the appropriate phase factor of the wave function in order to fulfill the proper boundary conditions, one arrives at the eigenvalue problem (for details see Ref. [8])

$$\tilde{H}(R,\omega)\Phi_j(\mathbf{q},R,\omega) = \tilde{E}_j(R,\omega)\Phi_j(\mathbf{q},R,\omega), \tag{10}$$

which determines the dynamical adiabatic eigenvalues and eigenfunctions. The effective "Hamiltonian" reads (in atomic units)

$$\begin{aligned}\tilde{H}(R,\omega) = &-\frac{1}{2}\Delta_q - R\left(\frac{Z_A}{|\mathbf{q} + \alpha\hat{\mathbf{q}}_1|} + \frac{Z_B}{|\mathbf{q} - \beta\hat{\mathbf{q}}_1|}\right) \\ &+ \omega L_3 + \frac{1}{2}\omega^2 q^2,\end{aligned} \tag{11}$$

where $\mathbf{q}$ is scaled electronic position vector, $Z_A$ and $Z_B$ are charges of the nuclei, $\alpha + \beta = 1$, $L_3$ is the component of the

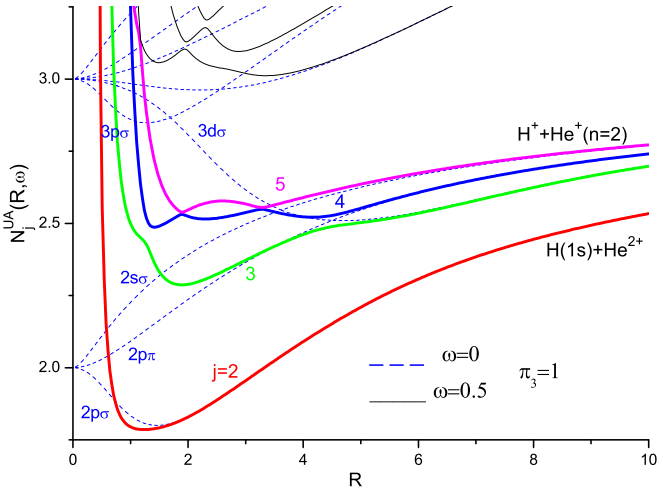


FIG. 1. (Color online) Segment of dynamical adiabatic eigenvalues for $\omega = 0.5$ represented in terms of the effective united-atom principal quantum number [Eq.(13); solid curves]. Also shown (dashed blue curves) are the standard adiabatic eigenvalues of the $(HeH)^{2+}$ molecular ion labeled by united-atom quantum numbers. $N_j^{UA}(R,\omega)$ is dimensionless, and other quantities are in atomic units.

electronic angular momentum along the $\hat{\mathbf{q}}_3$ axis (perpendicular to the scattering plane), and $\omega = bv$. The attribute dynamical" for eigenvalues and eigenfunctions comes from the fact that, besides the internuclear separation $R$, they depend on $\omega$, which is a parameter related to the dynamics of the nuclei. In contrast to the adiabatic approximation (corresponding to the two-Coulomb-center problem) the eigenvalue problem (10) is not separable. The only symmetry which we have in this case is the parity $\Pi_3 = \pm 1$ with respect to the reflection $q_3 \to -q_3$. The adiabatic eigenvalues $E_j(R)$ and dynamical adiabatic eigenvalues $\tilde{E}_j(R,\omega)$ are related by the expression

$$E_j(R) = \tilde{E}_j(R,\omega \to 0)/R^2. \tag{12}$$

General properties of the dynamical adiabatic eigenvalues for real values of $R$ ranging from $R = 0$ (united-atom limit) to $R \to \infty$ (separated-atom limit) have been discussed in detail in Ref. [8]. For a graphical representation of the $R$ dependence of the eigenvalues it is more convenient to use the "effective united-atom principal quantum number,"

$$N_j^{UA}(R,\omega) = (Z_A + Z_B)[-2\tilde{E}_j(R,\omega)/R^2]^{-1/2}. \tag{13}$$

Figure 1 shows this quantity for the $(HeH)^{2+}$ system for two cases: $\omega = 0$ (standard adiabatic curves; dashed curves labeled by the united-atom quantum numbers) and $\omega = 0.5$ a.u. (dynamical adiabatic curves; solid lines labeled $j = 2,3,\ldots$). One can see that at large internuclear separations the two sets of eigenvalues merge together. Note that the adiabatic curves exhibit a large number of exact crossings due to the high symmetry (separability) of the two-Coulomb-center problem. By introduction of the two last terms in Eq. (11) this symmetry is broken, and dynamical adiabatic curves exhibit only avoided crossings, although some of them can be very narrow. Four states labeled $j = 2$–5 are of particular interest in description of the process (1).

Analytic continuation of the dynamical eigenvalues into the complex $R$ plane was studied in Ref. [9]. Besides the usual hidden crossings responsible for electronic transitions due to the radial motion of the nuclei, a large number of the exact crossings between states of different symmetries in the two-Coulomb-center basis transforms into a new type of branch points which was called $L_3$ crossings and which was responsible for electronic transitions caused by the rotation of the internuclear axis. In this way, in the dynamical adiabatic theory, these two types of nonadiabatic transitions can be treated on equal footing. The transition probability related to any type of branch point is again determined by Eq. (4), but instead of adiabatic eigenvalues in Eq. (5) the dynamical adiabatic eigenvalues appear,

$$\Delta = \frac{1}{\hbar}\left|\mathrm{Im}\int_C \frac{\tilde{E}(R,\omega)}{R^2}\frac{dt}{dR}dR\right|. \tag{14}$$

In Ref. [9], the $\omega$ dependence of the positions in the complex $R$ plane of a number of hidden and $L_3$ crossings in the $(HeH)^{2+}$ system was analyzed. A more detailed analysis of branch points responsible for the charge-exchange process (1) will be presented in Sec. IV. But first, in the next section we shall concentrate on small internuclear separations where in the standard adiabatic approach the main transition mechanism of interest is the rotational coupling between the $2p\sigma$ and $2p\pi$ adiabatic states (see Fig. 1). It is of interest to investigate how this transition is described within the framework of the two-state dynamical adiabatic approximations introduced above via Eqs. (8) and (9).

## III. TWO-STATE UNITED-ATOM MODEL OF $2p\sigma$-$2p\pi$ COUPLING

At small internuclear separation $R$ the adiabatic states become spherically symmetry. In this region transitions between $2p\sigma$ and $2p\pi$ molecular orbitals can be described in an adiabatic basis by the system of equations (8) with the amatrix element of nonadiabatic coupling $W_1(R) = \omega\hbar/R^2$ and splitting between $2p\sigma$ and $2p\pi$ adiabatic energy levels $\Delta E_1(R) = \alpha\hbar R^2$, where $\alpha = 9/20$ a.u. in the case of the $(HeH)^{2+}$ system. After a scaling transformation to the dimensionless variable $\tau = vt/b$, the system of equations (8) takes the form

$$\begin{aligned} i\frac{d}{d\tau}g_\sigma(\tau) &= \frac{b_{sc}^3}{2}(1+\tau^2)g_\sigma(\tau) + \frac{1}{1+\tau^2}g_\pi(\tau), \\ i\frac{d}{d\tau}g_\pi(\tau) &= \frac{1}{1+\tau^2}g_\sigma(\tau) - \frac{b_{sc}^3}{2}(1+\tau^2)g_\pi(\tau), \end{aligned} \tag{15}$$

where $b_{sc} = \sqrt[3]{\alpha/v}b$ is the scaled impact parameter. Thus, the solution of the problem depends on a single dimensionless parameter $b_{sc}$. The adiabatic approximation for the system of equations (15) was developed in Refs. [15,16]. The specific feature of this problem is the linear dependence $\Delta E(R) \sim (\tau - \tau_c)$ in the vicinity of the complex crossing point $\tau_c = \pm i$. For that reason, Zwaan's method cannot be applied since, instead of three Stokes lines, there are four Stokes lines, and we lose control over the standard asymptote (3) during its continuation around the crossing point $\tau_c$. Here, a more complicated approach, based on the comparison

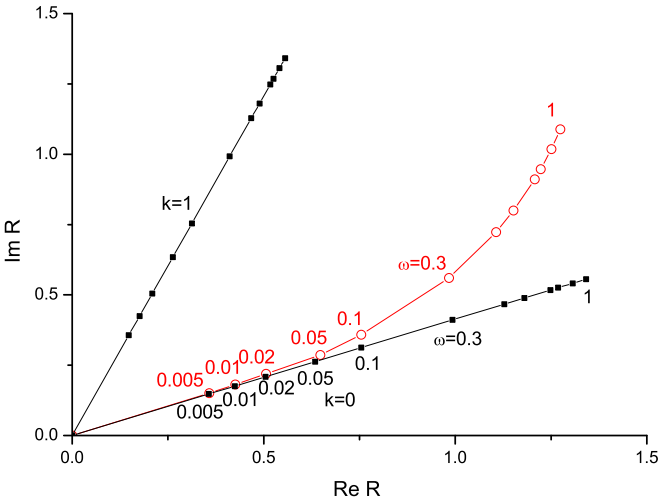


FIG. 2. (Color online) Trajectories of branch points relevant for the $2p\sigma$-$2p\pi$ transitions for increasing values of $\omega$. Black squares are for $k = 0$ and $k = 1$ branch points for the two-state model [Eq. (18)]. Red open circles are the exact calculation in the dynamical basis [9] corresponding to the $k = 0$ case. All quantities are in atomic units.

equation method, should be employed. The final expression for transition probability reads

$$P_{\rm ad} = 2e^{-2\Delta_{\rm ad}} = 2\exp\left(-\tfrac{4}{3}b_{\rm sc}^3\right), \tag{16}$$

where $\Delta_{\rm ad} = |{\rm Im}\int_0^{\tau_c}\Delta\mathcal{E}_1(R(\tau))d\tau|$ is the Stueckelberg parameter for the $\sigma$-$\pi$ transition and $\Delta\mathcal{E}_n(R(\tau)) = b\Delta E_n(R(\tau))/v\hbar$ $(n = 1,2,3)$ are the scaled energy splittings. For the sake of definiteness, a contour $C$ is chosen from $\tau = 0$ to $\tau = \tau_c$ and back. This expression differs by a factor of 2 from the general expression (4). In accordance with general theory, adiabatic wave functions $\varphi_\sigma(\mathbf{r},\tau)$ and $\varphi_\pi(\mathbf{r},\tau)$ coincide at $\tau = \tau_c$ (see Ref. [17], Sec. 3.2).

Some aspects of the dynamic approach to $2p\sigma$-$2p\pi$ transitions in the two-state model have been studied in Ref. [18]. In the first-order dynamical representation $(n = 2)$ the splitting of dynamical energy curves, according relations (9), reads

$$\Delta E_2(R) = \hbar\sqrt{\alpha^2R^4 + \frac{4\omega^2}{R^4}}. \tag{17}$$

This expression has eight branch points,

$$R_c = \sqrt[4]{2\omega/\alpha}e^{(2k+1)\pi i/8}, \quad k = 0,1,..,7. \tag{18}$$

In the physical region (Re $R \geqslant 0$) there are four of them. Figure 2 demonstrates trajectories of two branch points in the first quadrant of the complex $R$ plane. For comparison, in the $k = 0$ case the results of an exact calculation of branch points in the dynamical basis of the three-body problem [9] are also shown. In Figs. 3(a)–3(c) the scaled dynamical energy splitting $\Delta\mathcal{E}_2(R(\tau))$, the scaled matrix element of coupling $w_2(R(\tau)) = bW_2(R(\tau))/v\hbar$, and the Stokes lines are presented for $b_{\rm sc} = 0.7$. From Fig. 3(c) it is clear that the upper branch point $\tau_c(k = 1)$ has no physical meaning since it is separated from the real axis $R$ by the Stokes lines closest to the real-axis branch point $\tau_c(k = 0)$. Thus, the probability of inelastic transitions is determined by only the branch point $k = 0$. These transitions happen twice: during the approaching $(\tau_c = -\sqrt{R_c^2/b^2 - 1})$ and the receding $(\tau_c = +\sqrt{R_c^2/b^2 - 1})$ stages of collision. The total probability taking into account the interference between these two channels is

$$P_{\rm dyn} = 4e^{-2\Delta_{\rm dyn}}(1 - e^{-2\Delta_{\rm dyn}})\sin^2\phi_{\rm dyn}, \tag{19}$$

where $\Delta_{\rm dyn} = |{\rm Im}\int_0^{\tau_c}\Delta\mathcal{E}_2(R(\tau))d\tau|$ is the Stueckelberg parameter in the dynamical basis and $\phi_{\rm dyn} = |{\rm Re}\int_0^{\tau_c}\Delta\mathcal{E}_2(R(\tau))d\tau|$ is the phase shift between the upper and lower dynamical eigenenergy curves. Figure 4(a) shows the Stueckelberg parameters, and Fig. 4(b) shows phase shifts in the adiabatic and dynamical approaches as functions of scaled impact parameter $b_{\rm sc}$. As one can see from this figure, dynamical parameters approach adiabatic parameters in the limit $v \to 0$ $(b_{\rm sc} \to \infty)$. In the literature, sometimes the phase $\phi'_{\rm dyn} = |{\rm Re}\int_0^{{\rm Re}\tau_c}\Delta\mathcal{E}_2(R(\tau))d\tau|$ is employed (see, e.g., [19]). But Fig. 4(b) demonstrates that this choice is incorrect. Just as $\phi_{\rm dyn}$ tends in the limit $v \to 0$ to $\pi/4$, corresponding to adiabatic probability (16), the phase $\phi'_{\rm dyn}$ is very far from the $\pi/4$ limit. In Fig. 5 the probability of $\sigma$-$\pi$ transition as a function of the scaled impact parameter $b_{\rm sc}$ obtained in both the adiabatic (16) and the dynamic (19) bases is compared with the numerical solution of the system of equations (15). The adiabatic region corresponds to large values of the scaled impact parameter. As one can see, the dynamical approach essentially improves the agreement with the exact calculation. In Fig. 5 the probability of the $\sigma$-$\pi$ transition including the phase shift coming from the next order of adiabatic approximation in terms of the confluent hypergeometric comparison equation [19]

$$\chi_{\rm dyn} = \frac{\pi}{4} - \frac{1}{\pi}\Delta_{\rm dyn} + \frac{1}{\pi}\Delta_{\rm dyn}\log\left(\frac{1}{\pi}\Delta_{\rm dyn}\right) - \Gamma\left(1 + \frac{i}{\pi}\Delta_{\rm dyn}\right) \tag{20}$$

is also plotted. Here, the phase $\varphi_{\rm dyn}$ in Eq. (19) should be replaced by $\varphi_{\rm dyn} + \chi_{\rm dyn}$. On one hand, this correction does not change the result in the adiabatic limit since $\chi_{\rm dyn} \sim v \to 0$, but on the other hand, it essentially reduces the region of validity, giving the artificial nonphysical structure. Thus, its inclusion is useless in practice, and adiabatic approximation has the widest region of validity in the leading order, as it follows from the general theory of asymptotic expansions.

Now let us examine the next order of dynamical approach $n = 3$ obtained from relations (9). Figures 3(d)–3(f) illustrate the scaled dynamical energy splitting $\Delta\mathcal{E}_3(R(\tau))$, the scaled matrix element of coupling $w_3(R(\tau))$, and the Stokes lines, all for the case of the scaled impact parameter $b_{\rm sc} = 0.7$. In this basis two different branch points contribute to $\sigma$-$\pi$ transitions, $\tau_{c1}$ and $\tau_{c2}$. The total amplitude of the transition can be obtained from the transient matrix

$$\widehat{U} = \widehat{U}_2^{(+)}\widehat{U}_1^{(+)}\widehat{U}_1^{(-)}\widehat{U}_2^{(-)}, \tag{21}$$

where

$$\widehat{U}_i^{(\pm)} = \begin{pmatrix} \sqrt{1-p_i} & \sqrt{p_i}e^{\pm i\phi_i \pm i\pi/2} \\ \sqrt{p_i}e^{\mp i\phi_i \pm i\pi/2} & \sqrt{1-p_i} \end{pmatrix} \tag{22}$$

is the transient matrix due to the $\tau_{ci}$ branch point, $p_i = \exp(-2\Delta_i)$, $\Delta_i = |{\rm Im}\int_0^{\tau_{ci}}\Delta\mathcal{E}_3(R(\tau))d\tau|$,

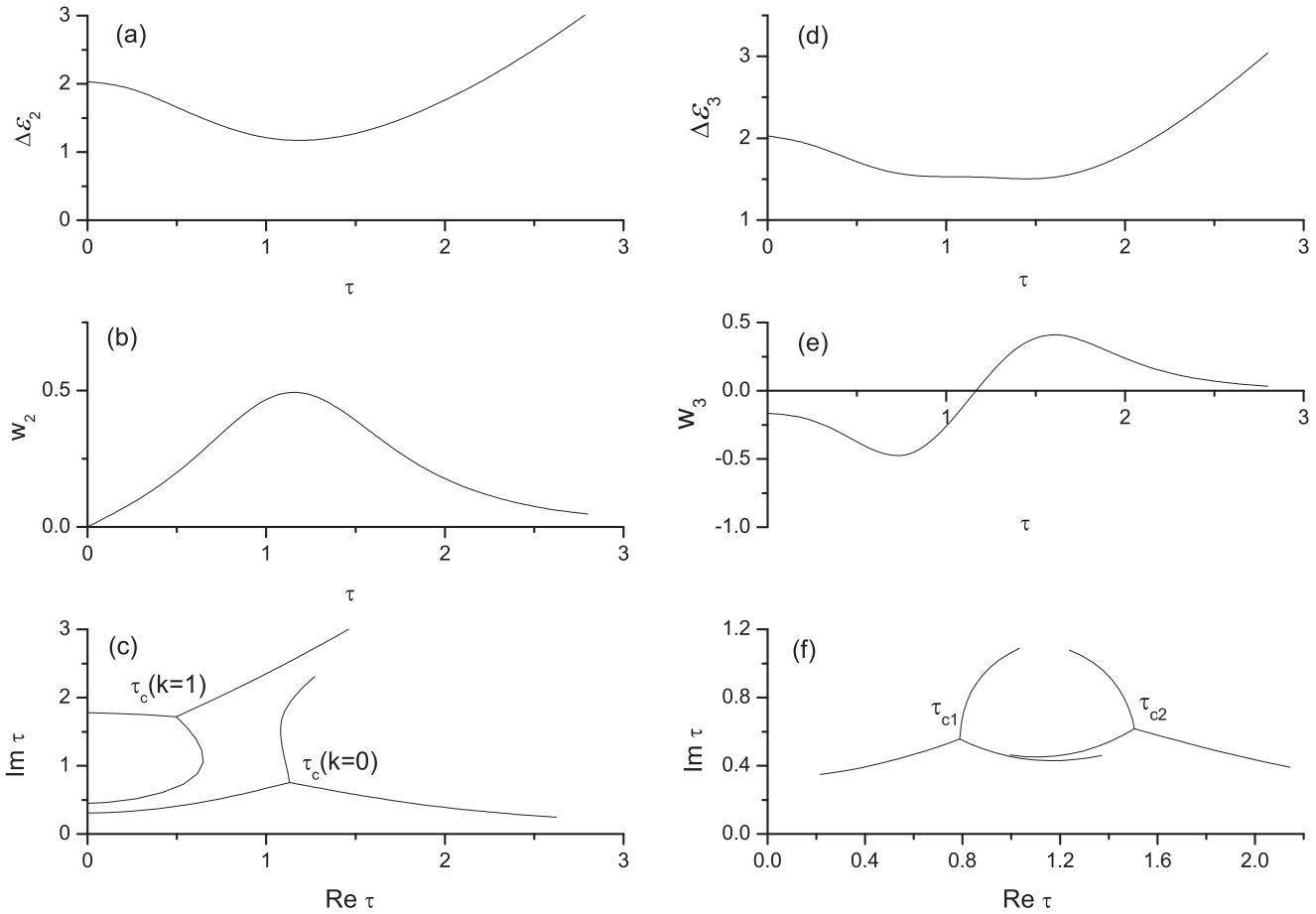


FIG. 3. (a), (d) Scaled dynamical energy splittings $\Delta\mathcal{E}_n(R(\tau)) = b\Delta E_n(R(\tau))/v\hbar$, $n = 2,3$. (b), (e) Scaled matrix elements of coupling $w_n(R(t)) = bW_n(R(\tau))/v\hbar$, $n = 2,3$. (c), (f) Branch points and Stokes lines. $\tau = vt/b$ is the scaled time variable, and in all cases the scaled impact parameter $b_{sc} = 0.7$. All quantities are dimensionless.

$\phi_i = |\mathrm{Re}\int_0^{\tau_{ci}} \Delta\mathcal{E}_3(R(\tau))d\tau|$, and $\widehat{U}_i^{(+)}$ and $\widehat{U}_i^{(-)}$ describe, respectively, the transition during the receding and approaching stages of collision. The topological phase $\pi/2$ in the nondiagonal matrix elements of $\widehat{U}_i$ comes from the singular factor in basis eigenfunction (7). The expression for the $\sigma$-$\pi$ transition probability is

$$P(\tau_1,\tau_2) = 4|\{(1-p_1)\sqrt{p_2(1-p_2)}\sin\phi_2 + p_1\sqrt{p_2(1-p_2)}\sin(\phi_2-2\phi_1) + (1-2p_2)\sqrt{p_1(1-p_1)}\sin\phi_1\}|^2. \quad (23)$$

Figure 6 shows the probabilities of the $\sigma$-$\pi$ transition via the $\tau_{c1}$ and $\tau_{c2}$ branch points separately and via both channels. In the adiabatic limit $b_{sc} \to \infty$ the total probability approaches the exact result but slower than in the previous dynamical basis $n = 2$. At $b_{sc} < 1$ a.u. transitions via the $\tau_{c1}$ and $\tau_{c2}$ branch points compensate each other since the matrix element of nonadiabatic coupling $W_3(R)$ has opposite sign in the vicinity of $\mathrm{Re}(\tau_{c1})$ and $\mathrm{Re}(\tau_{c2})$ [see Fig. 3(e)]. From Fig. 6 it is clear that the dynamical approach of higher order ($n = 3$), as well as the phase shift from the next order of adiabatic expansion (20), worsens the agreement with accurate numerical results, and there is no sense in applying it in practice.

## IV. CHARGE EXCHANGE IN COLLISIONS OF $He^{2+}$ WITH H(1*s*)

Referring to Fig. 1, the charge-exchange process (1) in the dynamical adiabatic basis corresponds to transitions from the initial $j_i = 2$ state to the final $j_f = 3,4,5$ states. The transitions can occur during the approaching stage of the collision (when $R$ decreases from $R = +\infty$ to $R = b$) as well as in the receding stage (when $R$ increases from $R = b$ to $R = +\infty$). Transition probabilities are predominantly determined by the distribution of those branch points in the complex $R$ plane which connects the analytic continuations of the dynamical adiabatic states with labels $j = 2$–5. The positions of these branch points, for the relevant ranges of the $\omega$ parameter, are shown in Fig. 7. Branch points are grouped in eight series labeled as $X(j_1 - j_2)$, where $X = L$, $P$, $R$, $Q$, $A$, $B$, $AB$, $C$ and $j_1, j_2 = 2$–5 indicate the labels of the dynamical adiabatic states which are (or are supposed to be) connected by the branch points. The series $L(2-3)$, $P(3-4)$, $R(3-4)$, and $Q(2-3)$ have already been discussed in Ref. [9] [with somewhat different respective notation: $L_3(2-3,4,5)$, $L_3(3-4)$, $L_3'(3-4)$, and $Q_1(2-3)$]. The series $A(4-5)$, $B(4-5)$, $AB(4-5)$, and $C(4-5)$ are presented here. Branch points belonging to the $Q(2-3)$ series correspond to the hidden-crossing type and are all located in the relatively small domain. $L(2-3)$, $P(3-4)$,

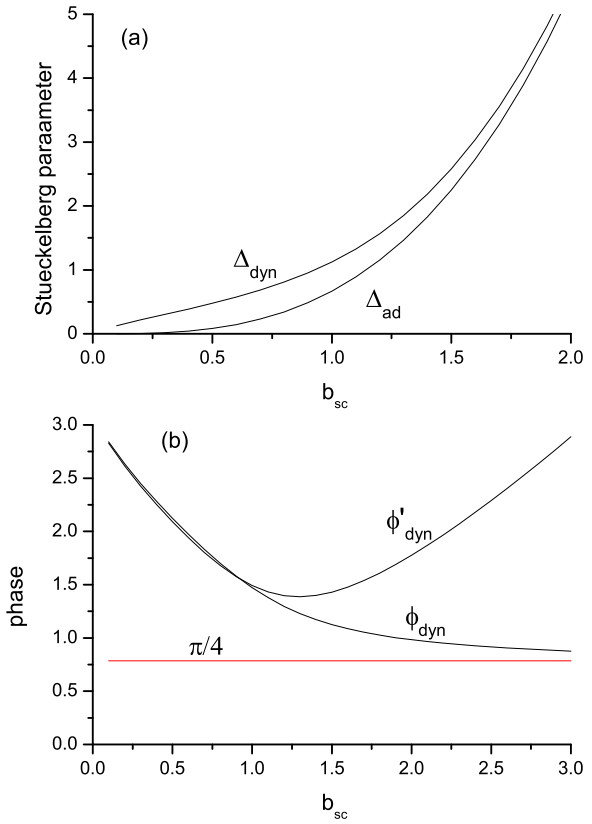


FIG. 4. (Color online) (a) Dimensionless Stueckelberg parameters and (b) phases calculated in adiabatic and dynamical bases as functions of the scaled impact parameter.

and $R(3-4)$ are all $L_3$ crossings; that is, they are related to the rotational coupling. While the $L(2-3)$ and $P(3-4)$ series originate from the united-atom degeneracies at $R=0$ for $\omega=0$, the $R(3-4)$ series originates from the exact crossing at $R=4.507$ a.u. for $\omega=0$ (between the $3d\sigma$ and $2p\pi$ adiabatic

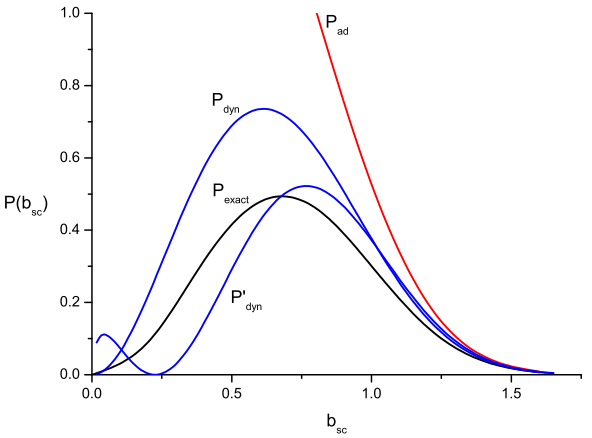


FIG. 5. (Color online) $\sigma$-$\pi$ transition probabilities: $P_{ad}$ is calculated using the adiabatic basis as given by Eq. (16). $P_{dyn}$ is calculated using the dynamical basis according to Eq. (19). $P'_{dyn}$ is the result obtainedby also using Eq. (19) but with additional phase $\chi$ as defined in Eq. (20), and $P_{exact}$ is the result of the numerical solution of the coupled equations (15).

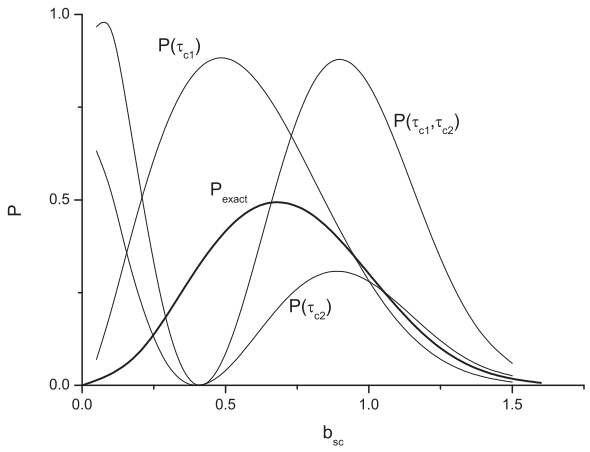


FIG. 6. Probabilities of $\sigma$-$\pi$ transitions as functions of the scaled impact parameter $b_{sc}$. The probabilities for transitions via the $\tau_{c1}$ and $\tau_{c2}$ branch points separately are labeled $P(\tau_{c1})$ and $P(\tau_{c2})$. The probability of transition via both channels simultaneously is labeled $P(\tau_{c1},\tau_{c2})$. $P_{exact}$ is the result of the numerical solution of the coupled equations (15)

curves, as seen in Fig. 1). As for the $A(4-5)$ and $C(4-5)$ series, they also seem to tend towards the origin when $\omega\to 0$, while the $B(4-5)$ series in this limit corresponds to the exact crossing at $R=3.616$ a.u. (between the $3d\sigma$ and $2s\sigma$ adiabatic curves, also visible in Fig. 1). The $AB(4-5)$ series is formed after $A(4-5)$ and $B(4-5)$ merge at the value of $\omega\approx 0.7$ a.u.

It is clear that taking into account all branch points and all possible transitions is a very complicated task. Consequently, we have made some simplifying assumptions. First of all, from Fig. 7 it is clear that for the wide range of $\omega$ values the imaginary parts of the branch points in the $C(4-5)$ series are very small. Therefore, we have assumed that the

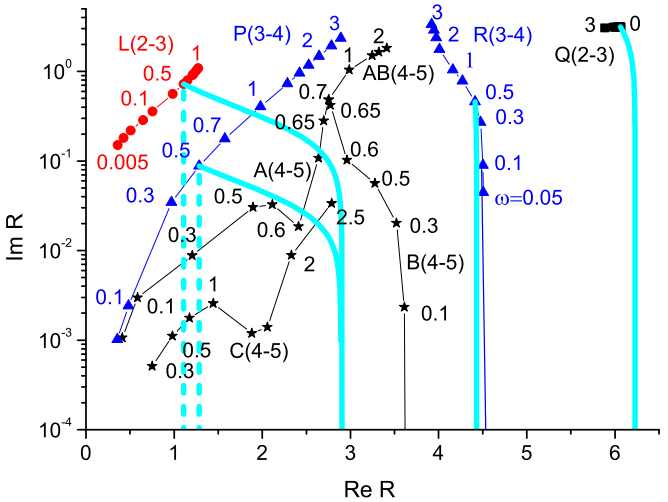


FIG. 7. (Color online) Positions of branch points belonging to series $X(j_1-j_2), X=L, P, R, Q, A, B, AB, C$ and connecting the dynamical eigenvalues labeled with $j_1, j_2=2$–5 for various values of the $\omega$ parameter. Thick cyan lines represent integration paths for calculation of the Stueckelberg parameters for the case of $v=0.173$ and $\omega=0.5$. All quantities are in atomic units

corresponding very narrow avoided crossings are always passed diabatically. The same is also true for the $A(4-5)$ and $B(4-5)$ series, at least for not too large values of $\omega$. For example, in Fig. 1 for $\omega = 0.5$ a.u., two narrow avoided crossings corresponding to $A(4-5)$ and $B(4-5)$ branch points can clearly be seen. Treating them as exact crossings leads then to simply redefining state $j = 5$ to play the role of state $j = 4$ in the $R$ interval between the diabatic crossings. The role of the $AB(4-5)$ series was neglected on the grounds that it appears at relatively large values of $\omega$, corresponding to larger values of the impact parameter where the transitions are mainly governed by the two outer series: $R(3-4)$ and $Q(2-3)$. In this way we have effectively excluded state $j = 5$ from consideration, and the charge-exchange process (1) will be described by calculating the probabilities of the $j_i = 2 \to j_f = 3$ and $j_i = 2 \to j_f = 4$ transitions caused by the presence of branch points in series $L(2-3)$, $P(3-4)$, $R(3-4)$, and $Q(2-3)$.

For fixed relative collision velocity and a fixed impact parameter, $\omega = vb$ is also fixed, and we deal with four branch points in the first quadrant of the complex $R$ plane which we can label as $R_X$, where $X = L, P, R, Q$ indicates the above-discussed series. In the fourth quadrant there are the complex-conjugate branch points $R_X^*$ which connect the complex-conjugate dynamical adiabatic eigenvalues $\tilde{E}_j^*(R,\omega)$. Through the mapping $t = \pm\sqrt{R^2 - b^2}/v$, for each $R_X$ we find in the first quadrant of the complex $t$ plane the branch point $t_X$ and in the second quadrant the branch point $-t_X^*$. A schematic representation (without real scaling of distances) of the typical distribution of branch points in the upper half of the complex $t$ plane is shown in Fig. 8.

The probabilities of the $j_i = 2 \to j_f = 3$ and $j_i = 2 \to j_f = 4$ transitions are calculated by summing up coherently all complex probability amplitudes containing phase integrals of the dynamical adiabatic eigenvalues along all possible paths $C_{j_i,j_f}^{(k)}$ in the upper half of the complex $t$ plane that start at $t \to -\infty$ in the initial $j_i = 2$ state, encircle a certain number of branch points, and end up in either the $j_f = 3$ or $j_f = 4$ state for $t \to +\infty$ [20]:

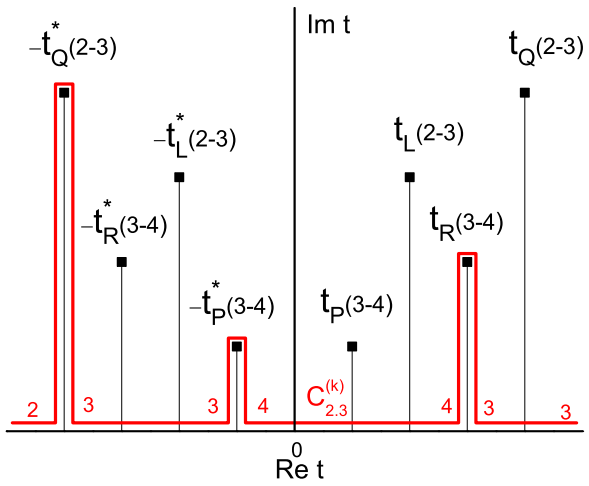


FIG. 8. (Color online) Schematic representation of positions of the branch points in the upper half of the complex $t$ plane. The typical path $C_{2,3}^{(k)}$ contributing to the $2 \to 3$ transition is shown.

$$P_{j_i,j_f} = \left| \sum_{k=1}^{N_{j_i,j_f}} A_{j_i,j_f}^{(k)} \exp\left\{ -i\phi_{j_i,j_f}^{(k)} - in_{j_i,j_f}^{(k)}\pi/2 \right\} \right|^2, \quad (24)$$

where $N_{j_i,j_f}$ is the total number of paths (in our case we find $N_{2,3} = 22$ and $N_{2,4} = 14$). Phases are given by

$$\phi_{j_i,j_f}^{(k)} = \frac{1}{\hbar}\mathrm{Re}\int_{C_{j_i,j_f}^{(k)}} \frac{\tilde{E}(R,\omega)}{R^2}dt, \quad (25)$$

and $n_{j_i,j_f}^{(k)}$ is a whole number equal to the difference of the number of times the branch points have been encircled in the approaching (Re $t < 0$) and receding (Re $t > 0$) parts of the collision (each encircling contributes a "topological phase" of $\mp\pi/2$ [20]). For the particular example of a $C_{2,3}^{(k)}$ path shown in Fig. 8, we find $n_{2,3}^{(k)} = 1$. Amplitudes $A_{j_i,j_f}^{(k)}$ are the products of a certain number of terms of the form $\sqrt{p_X}$ or $\sqrt{1-p_X}$ ($X = L, P, R, Q$) which appear depending on whether along the path a single-pass transition related to the branch point $X$ is either possible and occurs or possible but does not occur. For example, for the path shown in Fig. 8 we find

$$A_{2,3}^{(k)} = \sqrt{p_Q}\sqrt{1-p_R}\sqrt{1-p_L}\sqrt{p_P}\sqrt{1-p_P}\sqrt{p_R}\sqrt{1-p_Q}. \quad (26)$$

Single-pass transition probabilities $p_X$ are defined according to Eqs. (4) and (14):

$$p_X = e^{-2\Delta_X}, \quad (27)$$

where

$$\Delta_X = \frac{1}{\hbar}\left|\mathrm{Im}\int_{C_X} \frac{\tilde{E}(R,\omega)}{R^2}dt\right| \quad (28)$$

and $C_X$ is a contour which encircles the branch point $t_X$ (or $-t_X^*$) starting and ending at the real $t$ axis (three such vertical contours can be seen along the path shown in Fig. 8).

For the two cases of relative collision velocities $v = 0.173$ a.u. and $v = 0.283$ a.u. considered in the present work, the impact parameter dependencies of Stueckelberg parameters $\Delta_X$ and single-pass transition probabilities $p_X$ for four series of branch points ($X = P, L, R, Q$) are shown in Fig. 9. While these quantities in the cases of the $L, R$, and $Q$ series exhibit more or less expected behavior ($L$-branch points are operational at small impact parameters, $R$-branch points are operational at intermediate values, and $Q$-branch points affect transition in the whole range), the nonmonotonic behavior of $\Delta_P$ and $p_P$ is rather surprising. Therefore, we discuss below in some detail how these quantities are calculated.

In practice, the integral in Eq. (29) is calculated for each branch point $t_X(j_1 - j_2)$ as

$$\int_{C_X} \frac{\tilde{E}(R,\omega)}{R^2}dt = \int_{\mathrm{Re}\,t_X}^{t_X} \frac{\tilde{E}_{j_1}(R,\omega) - \tilde{E}_{j_2}(R,\omega)}{R^2}dt \quad (29)$$

that is, as an integral along one of the four vertical straight lines in the first quadrant of the schematic representation in Fig. 8. In reality, these four straight lines are mapped into four curved lines in the first quadrant of the complex $R$ plane. For the case

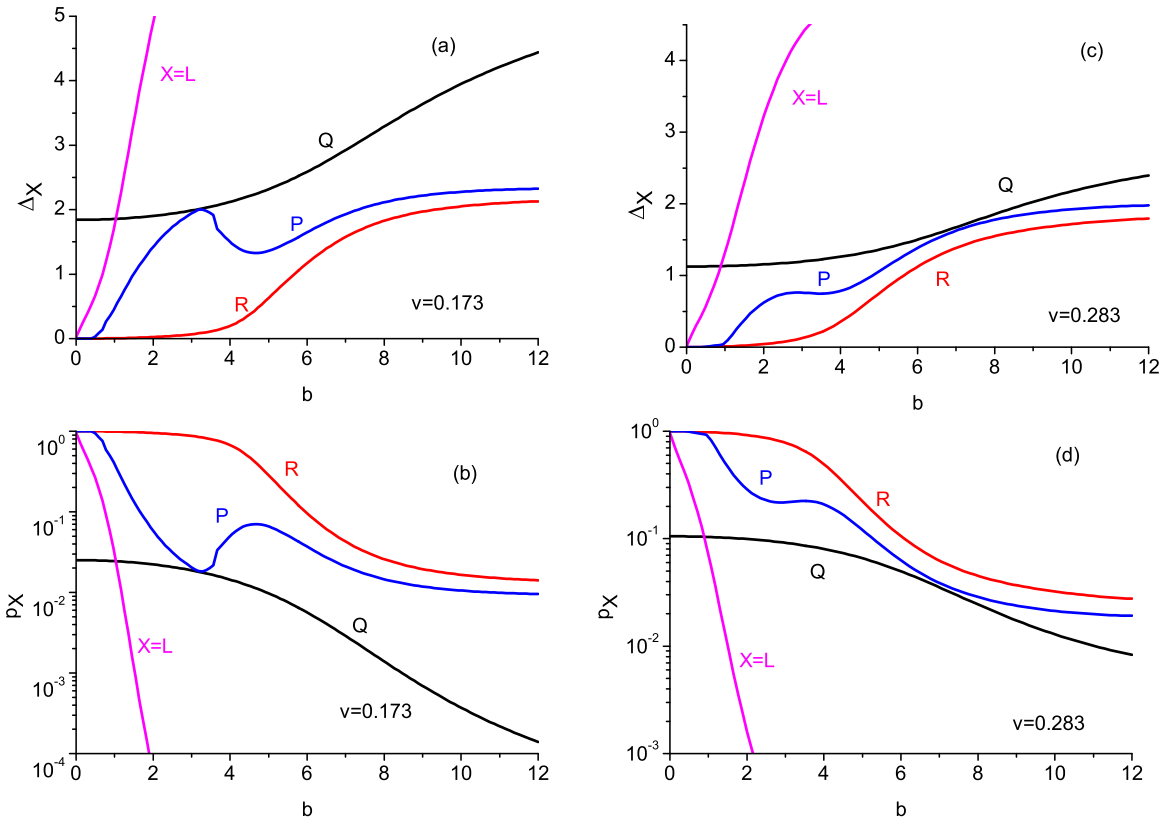


FIG. 9. (Color online) Stueckelberg parameters $\Delta_X$ and single-pass probabilities $p_X$ as functions of impact parameter for two values of the impact velocities. $\Delta_X$ and $p_X$ are dimensionless, and other quantities are in atomic units.

of $v = 0.173$ a.u., $\omega = 0.5$ a.u. (which implies $b = 2.89$ a.u.), these curves are shown in Fig. 7 as thick cyan lines. Each of these curves starts on the real axis at $R = \sqrt{b^2 + (v\mathrm{Re}\, t_X)^2}$ and ends up at the branch point $R_X$ [a member of the $X(j_1 - j_2)$ series labeled with $\omega = 0.5$ a.u.].

We have verified that when one starts with eigenvalues labeled with $j_1 = 2$ and $j_2 = 3$ on the real axis and analytically continues these eigenvalues along the path shown in Fig. 7 as the solid thick line which ends up at $R_L$, indeed, the branch-point singularity is reached. It is of interest to note that this is seemingly in contrast to the assignment from our previous work [9], in which it was found that this branch point connects the analytic continuations of eigenvalues labeled with $j_1 = 2$ and $j_2 = 4$. The reason for this is because in Ref. [9] the path of analytic continuation was the vertical straight line from $R = \mathrm{Re}R_L$ to $R = R_L$, shown in Fig. 7 as a thick dashed line. Why the two assignments differ becomes clear when one notices that the contour formed by the solid and dashed lines which join at $R_L$ encircle the branch point $R_P$ [the member of the $P(3-4)$ series labeled with $\omega = 0.5$ a.u.]. We have also verified that for all other members of the $L$ series the assignment $L(2-3)$ in the above sense is correct. Anyway, the correct labels of states coupled by the given branch point $t_X$ are determined along the vertical line from Re $t_X$ to $t_X$ in only the complex $t$ plane.

Unfortunately, similar reasons lead to the result that when the analytic continuation is performed along the path shown in Fig. 7 as a solid thick line which ends up at $R_P$, this branch point connects the eigenvalues labeled at the real $R$ axis with $j_1 = 3$ and $j_2 = 5$, which violates the assignment $P(3-4)$ of the $P$ series. Again, this is due to the fact that, as seen in Fig. 7, the contour formed by the solid and dashed lines which join at $R_P$ encircles the branch point $R_A$ [the member of the $A(4-5)$ series labeled with $\omega = 0.5$ a.u.]. The same problem arises for all branch points of the $P$ series with $\omega =$ 0.2–0.6 a.u. Outside this interval the assignment $P(3-4)$ is not violated. An accurate solution of this problem requires the use of the comparison equation with two branch points passing each other. But, to our knowledge, such a solvable equation is not known. That is why the calculations have been completed using values of $\Delta_P$ shown in Fig. 9, which were calculated using Eq. (29) with $j_1 = 3$ and $j_2 = 4$. As for the $R(3-4)$ and $Q(2-3)$ series of branch points we have not detected any problems of this kind.

For the case of the relative collision velocity of $v = 0.173$ a.u. the weighted probabilities $bP_{2,3}$, $bP_{2,4}$, and $b(P_{2,3} + P_{2,4})$ as functions of the impact parameter $b$ have been calculated using Eq. (24) and are shown in Fig. 10. $P_{2,4}$ exhibits a large peak at small impact parameters due to the contribution of the $L(2-3)$ series and a smaller peak at intermediate impact parameters due to the contributions of the $P(3-4)$ and $R(3-4)$ series of branch points. $P_{2,3}$ contributes the overall interference structure (Stueckelberg oscillations) mainly due to the $Q(2-3)$ series of branch points. Also shown in Fig. 10 are the results of hyperspherical close-coupling calculations [3]. Overall agreement with our results is satisfactory, except that we are missing the structured peak located around $b \approx 1.5$ a.u. The sources of this disagreement can be various; the possible

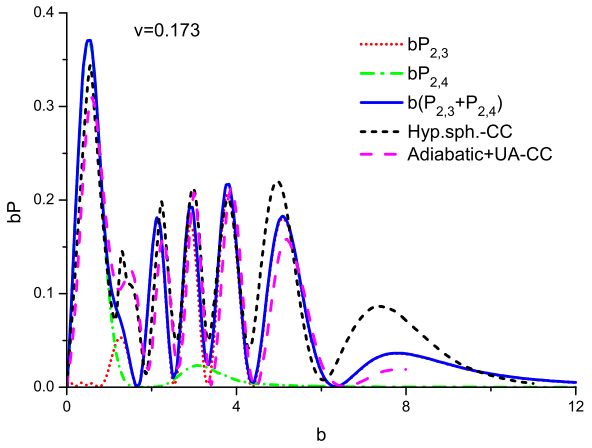


FIG. 10. (Color online) Weighted electron-capture probabilities as functions of the impact parameters at relative collision velocity $v = 0.173$. Dotted curve: $j_i = 2 \rightarrow j_f = 3$ transitions, dash-dotted curve: $j_i = 2 \rightarrow j_f = 4$ transitions, solid curve: total electron transfer. The short-dashed curve corresponds to the total probability of hyperspherical close-coupling calculations [3]. The long-dashed curve is the result of the adiabatic approach combined with united-atom close-coupling calculations in order to include the first peak [20,21]. All quantities are in atomic units.

one is our exclusion of the $j = 5$ state from the considerations. Also shown in Fig. 10 are the results of the combination of the standard adiabatic (hidden crossing) theory and the united-atom close-coupling (UA-CC) calculation [20,21]. The adiabatic approach is able to reproduce only the oscillatory structure as it originates from the radial coupling. The first large peak at small impact parameters originates from the $2p\sigma$-$2p\pi$ rotational coupling close to the united-atom limit and could be reproduced only by adding the results of the close-coupling calculations. In addition, this method does not take into account the rotational transitions due to exact crossing between the $2p\pi$ and $3d\sigma$ curves (see Fig. 1) and therefore does not reproduce the second small peak of the $j_i = 2 \rightarrow j_f = 4$ transitions present in the results of the dynamical adiabatic approach.

Figure 11 shows the weighted probabilities at somewhat higher collision velocity $v = 0.283$ a.u. Here, the rotational peak at small impact parameters is no longer dominant with respect to the Stueckelberg oscillations, and rotational peak at intermediate impact parameters is smoothed out. A comparison with the results of hyperspherical close-coupling calculations indicates that our method predicts a slower

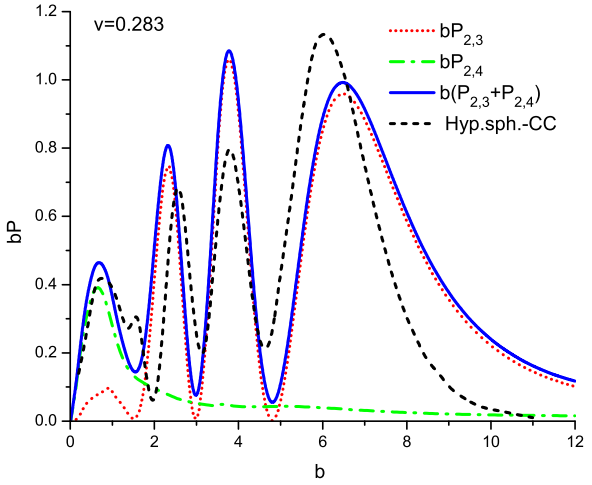


FIG. 11. (Color online) Same as Fig. 10, but for the relative collision velocity of $v = 0.283$.

decrease of the electron-capture probability at large impact parameters.

## V. CONCLUDING REMARKS

The application of dynamical adiabatic theory for describing electronic transitions in ion-atom collisions is more complicated than the standard adiabatic theory. This is because one has to deal with a series of branch points in the complex $R$ plane which change their positions when dynamical parameters (such as $\omega = bv$) are changed. On the other hand, the great advantage of this method is that electronic transitions caused by the relative radial and angular motion of the nuclei can be treated on equal footing, a property which is missing in the standard adiabatic approach. As the comparison with the results of very elaborate calculations (such as hyperspherical close-coupling method) shows, the precision of the method is satisfactory. In addition, it allows for interpretation of the results in terms of various transition mechanisms related to particular types of branch points.

## ACKNOWLEDGMENTS

This work was partly supported by the Serbia-JINR collaboration program. T.P.G. acknowledges the support from the Ministry of Education, Science and Technological Development of the Republic of Serbia through Project No. 171020. We are indebted to R. McCarroll for critical reading of the manuscript.

[1] R. McCarroll and D. S. F. Crothers, Adv. At. Mol. Opt. Phys. **32**, 253 (1994).
[2] J. Macek, J. Phys. B **1**, 831 (1968).
[3] C.-N. Liu, A.-T. Le, T. Morishita, B. D. Esry, and C. D. Lin, Phys. Rev. A **67**, 052705 (2003).
[4] E. A. Solov'ev, Theor. Mat. Phys. **28**, 757 (1976).
[5] V. V. Serov, V. L. Derbov, B. B. Joulakian, and S. I. Vinitsky, Phys. Rev. A **75**, 012715 (2007).
[6] E. Y. Sidky and B. D. Esry, Phys. Rev. Lett. **85**, 5086 (2000).
[7] A. Hamido, J. Eiglsperger, J. Madronero, F. Mota-Furtado, P. O'Mahony, A. L. Frapiccini, and B. Piraux, Phys. Rev. A **84**, 013422 (2011).
[8] T. P. Grozdanov and E. A. Solov'ev, Phys. Rev. A **88**, 022707 (2013).
[9] T. P. Grozdanov and E. A. Solov'ev, Phys. Rev. A **90**, 032706 (2014).

[10] M. Born and V. A. Fock, Z. Phys. **51**, 165 (1928).
[11] E. C. G. Stueckelberg, Helv. Phys. Acta **5**, 369 (1932).
[12] A. Zwaan, Arch. Neerl. Sci. Exactes Nat., Ser. IIIA **12**, 1 (1929).
[13] L. D. Landau and E. M. Lifshitz, *Quantum Mechanics* (Pergamon, Oxford, 1965).
[14] Y. N. Demkov, V. N. Ostrovskii, and E. A. Solov'ev, Phys. Rev. A **18**, 2089 (1978).
[15] E. A. Solov'ev, Vestn. Leningr. Univ. Fiz. Khim. **4**, 10 (1976).
[16] A. I. Voronin, S. P. Karkach, V. I. Osherov, and V. G. Ushakov, Sov. Phys. JETP. **44**, 465 (1976).
[17] E. A. Solov'ev, Sov. Phys. Usp. **32**, 228 (1989).
[18] H. Nakamura and M. Namiki, Phys. Rev. A **24**, 2963 (1981).
[19] J. E. Bayfield, E. E. Nikitin, and A. I. Reznikov, Chem. Phys. Lett. **19**, 471 (1973).
[20] R. K. Janev, J. Pop-Jordanov, and E. A. Solovev, J. Phys. B **30**, L353 (1997).
[21] E. A. Solov'ev, J. Phys. B **38**, R153 (2005).